Applied Physics Letters ARTICLE pubs.aip.org/aip/apl

Space charge-induced capacitance recovery in blue quantum dot light-emitting diodes

Cite as: Appl. Phys. Lett. **125**, 113502 (2024); doi: 10.1063/5.0226752
Submitted: 3 July 2024 · Accepted: 30 August 2024 ·
Published Online: 10 September 2024

Xiangwei Qu,[1,2] Jingrui Ma,[1,2] Depeng Li,[1,2] Kai Wang,[1,2] and Xiao Wei Sun[1,2,a)]

AFFILIATIONS

[1]Institute of Nanoscience and Applications, and Department of Electrical and Electronic Engineering, Southern University of Science and Technology, Shenzhen 518055, China
[2]Key Laboratory of Energy Conversion and Storage Technologies (Southern University of Science and Technology), Ministry of Education, and Shenzhen Key Laboratory for Advanced Quantum Dot Displays and Lighting, Southern University of Science and Technology, Shenzhen 518055, China

[a)]Author to whom correspondence should be addressed: sunxw@sustech.edu.cn

ABSTRACT

In this work, we report the capacitance recovery behavior in the blue quantum dot light-emitting diode (QLED) by capacitance–voltage (C–V) characterizations. A comprehensive study of the C–V, dC/dV–V, and current density–voltage characteristics of pristine and shelf-aged devices suggests that capacitance recovery is associated with space charge-induced charge accumulation. At lower temperatures, the capacitance recovery in the shelf-aged device is efficiently suppressed due to the difficulty in building up the space charge, which supports our argument. Moreover, the capacitance recovery behavior of QLED only happens at low frequencies (a few hundred hertz), which is related to the time constant for charge accumulation at the selected voltage. Our work shows the effect of space charge on device capacitance and enriches the comprehension of carrier processes in QLED under AC measurement.

Owing to narrow linewidth, high performance, and cost-effective manufacturing, quantum dot light-emitting diode (QLED) is regarded as a strong candidate for the next generation displays.[1–6] In a working device, once the applied bias is added on a QLED, electrons are injected from cathode and transport through the electron transport layer (ETL) into the quantum dot (QD) layer. Simultaneously, holes are injected from the anode into the hole injection layer (HIL), and then travel through the hole transport layer (HTL) into the QD layer. Subsequently, electrons and holes form excitons in the QD layer. Finally, photons are generated by radiative recombination of exciton and escape the device.[6] Therefore, the fundamental carrier processes including charge injection and transport, as well as exciton recombination, can significantly affect the performance of QLEDs. Particularly, the charge injection process plays an important role in achieving a balanced charge injection, while the exciton recombination process determines the luminance efficiency. A number of strategies have been evolved to realize a balance in charge injection and enhancing luminance efficiency,[1–5] thus boosting the electroluminescent efficiency of QLED. However, the charge dynamics of QLED, such as charge injection and exciton dissociation mechanisms,[4,7–9] remain unclear.

Impedance spectroscopy (IS) is a useful tool to provide physical insight into carrier processes of QLED[10–17] since it reflects an electrical response of the material, interface, and the whole device to an alternating voltage. Among the characteristic curves of IS, Nyquist plot plays a significant role in constructing an equivalent circuit model of QLED.[11,12] The capacitance–frequency (C–f) characteristics are commonly employed to calculate the trap distribution if the capacitance raise only resulted from the carrier trapping process.[13,14] However, these characteristic curves can only procure the electrical parameters of QLED at a selected voltage. To better depict the carrier processes across a wide voltage range, a capacitance–voltage (C–V) characteristic can track the working point in a current density–voltage (J–V) characteristic throughout a large voltage range.[10,15–17] Generally, an increase in capacitance above geometrical capacitance (C_g) stems from charge accumulation, while a drop in capacitance results from charge recombination, which consumes the free carrier. This indicates a direct correlation of capacitance to changes in the amount of charge.[16] Therefore, the C–V curve is useful to illustrate the charge accumulation and recombination processes in QLED. In addition, the derived dC/dV–V characteristic is developed to evaluate the charge accumulation or recombination rate in detail,[18,19] providing an in-depth understanding of the carrier processes.

In a typical C–V curve in QLED, the device capacitance remains constant at low bias. After the device is turned on, the capacitance

increases as the applied voltage rises. Once it reaches its peak value, the capacitance begins to decrease, eventually leading to a negative capacitance. Some works have noted unusual capacitance recovery at negative capacitance,[18–22] yet its origin is rarely discussed. In this work, we report the capacitance recovery behavior and its underlying origin in blue QLED. Comparing the C–V characteristics of both pristine and shelf-aged blue QLEDs, we identify that the capacitive recovery behavior is only exhibited in the shelf-aged device. Further investigation of C–V, dC/dV–V, and J–V characteristics of both devices provides us insight into the capacitive recovery behavior, which could be linked to space charge-induced charge accumulation. Interestingly, the capacitance recovery behavior can be efficiently suppressed at lower temperatures, since it becomes challenging to establish the space charge. Moreover, the device capacitance recovery only happens at low frequency, which is associated with the time constant for charge accumulation. Our work shows the effect of space charge on the modulation of QLED capacitance.

Our QLED exhibits a pure blue emission at 467 nm (Fig. S1) with a structure of ITO/poly(3,4-ethylenedioxythiophene): polystyrene sulfonate (PEDOT:PSS)/poly(9,9-dioctylfluorene-co-N-(4-(3-methyl propyl)) diphenylamine) (TFB)/blue QD/ZnMgO/Al. Herein, ITO, PEDOT:PSS, TFB, blue QD, ZnMgO, and Al act as the anode, HIL, HTL, emission layer, ETL, and cathode in a QLED, respectively. Before device fabrication, ITO glasses were cleaned using a cleaning agent, followed by acetone, ethanol, and de-ionized water successively in an ultrasonic bath. After drying, ITO glasses were treated with oxygen plasma for 5 min. Then, the functional materials PEDOT:PSS, TFB, blue QD, ZnMgO were spin-coated on ITO glass layer by layer. After that, the ITO glasses were moved to a vacuum chamber for the deposition of an Al electrode. The resulting QLEDs were then encapsulated in a glovebox before conducting any electrical test. The J–V characteristics of blue QLED were measured by a dual-channel Keithley 2614B source measure unit. The C–V and C–f characteristics of blue QLEDs were measured using the Fluxim Paios measurement system with a 100 mV amplitude of the AC signal.

Figure 1(a) presents the C–V characteristics of pristine blue QLED at various frequencies, ranging from 100 Hz to 10 kHz. At 100 Hz, the device capacitance is contributed by C_g at low bias, which signifies little charge injection in blue QLED. As the voltage increases to V_t (2.2 V), there is a noticeable rise in capacitance, indicating the additional carrier generated by AC signal begins to inject into the device. After the characteristic voltage V_p at peak capacitance (2.7 V), the capacitance of blue QLED starts to drop, indicating charge recombination is dominant in the carrier process, which consumes the injected carriers. However, the characteristic voltages in the C–V curves are highly dependent on the applied frequency. Evidently, the V_t values in the C–V curve of pristine blue QLED increase to 2.4, 2.4, 2.6, and 2.7 V at frequencies of 500 Hz, 1kHz, 5 kHz, and 10 kHz, respectively. Similarly, the characteristic voltages V_p of the pristine device also increase to 2.8, 2.8, 2.9, and 2.9 V at the same applied frequencies. Therefore, it is not appropriate to depict the carrier processes according to the characteristic voltages.[23]

When the pristine blue QLED is stored in glovebox for one day, the feature of C–V characteristic is distinct from that of pristine device, especially at low frequency. As shown in Fig. 1(b), at 100 Hz, the capacitance of the shelf-aged device begins to rise at 2.2 V and achieves a peak value at 2.7 V. After that, the device capacitance starts to drop. However, at 3.1 V, the capacitance does not drop anymore, but it recovers from −6.48 to 14.24 nF when the voltage reaches 5.0 V. Likewise, at 500 Hz, the device capacitance recovery starts at 3.9 V (−6.0 nF), and it returns to −4.5 nF upon reaching 5.0 V. Meanwhile, the capacitance at 1 kHz starts to recover at 4.5 V, it can recover a little from −5.17 to −4.92 nF. The capacitance recovery behavior is also observed in red QLED (Fig. S3), which is consistent with that in blue QLED. Comparing with the C–V results, two key questions are left that need to be addressed: (i) the origin of capacitance recovery and (ii) why capacitance recovery only takes place at lower frequencies.

To uncover the origin of capacitance recovery of blue QLED, we have to analyze the charge distribution in pristine and shelf-aged devices. Generally, an increase in capacitance results from charge accumulation, while charge recombination would cause the capacitance to drop. Hence, the device capacitance represents the competition between charge accumulation and recombination processes, the device capacitance can be expressed as follows:[16]

$$C = \frac{dQ}{dV} = \frac{dQ_m + dQ_{acc} - dQ_r}{dv_{ac}}. \quad (1)$$

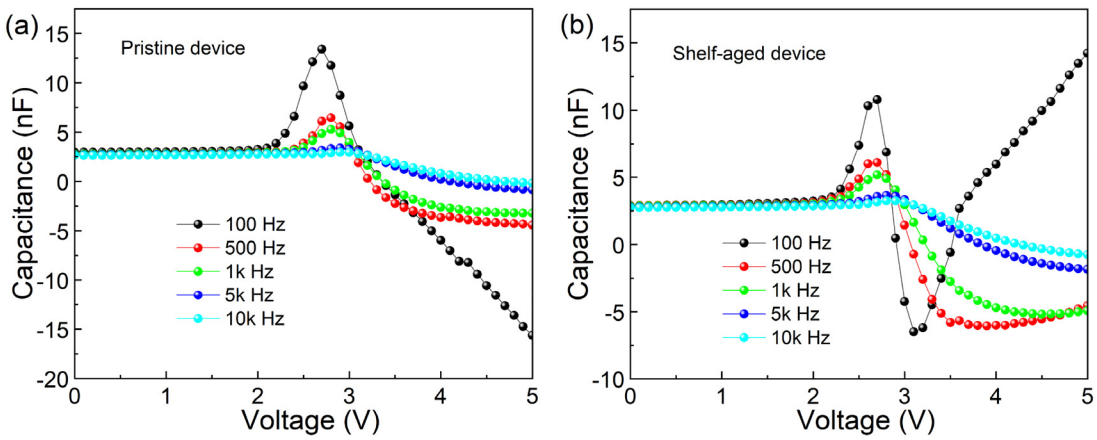

FIG. 1. Capacitance–voltage characteristics of (a) pristine and (b) shelf-aged device at various frequencies.

Here, Q represents the charge amount influenced by the AC signal perturbation v_{ac}, Q_m is the charge amount involved in electrode charging process, i.e., $Q_m = C_g v_{ac}$. Q_{acc} represents the accumulated charge amount, while Q_r is the charge amount depleted by charge recombination. According to Eq. (1), the capacitance above or below C_g reflects the competition between Q_{acc} and Q_r. On the other hand, the derived dC/dV–V characteristic is helpful for estimating the charge accumulation and recombination rates in detail.[18,19] Therefore, we link the C–V and dC/dV–V curves to interpret the capacitance recovery behavior in pristine and shelf-aged devices. As depicted in Fig. 2(a), the C–V and dC/dV–V curves of pristine blue QLED are separated into four regions, which correspond to different carrier processes. According to previous report, the carrier behaviors revealed by these curves is summarized as follows:[15–18]

1. In region I, where $C = C_g$, $dC/dV = 0$, there is little charge injection in device.
2. In region II, where $C > C_g$ and $dC/dV > 0$, Q_{acc} is larger than Q_r, which indicates charge accumulation is dominant in the carrier processes.
3. In region III, with $C > C_g$, $Q_{acc} > Q_r$, charge accumulation continues to dominate the carrier process. However, with $dC/dV < 0$, the charge accumulation rate decreases while the charge recombination rate increases in this region.
4. In region IV, $C < C_g$ and $dC/dV < 0$. Therefore, Q_{acc} is less than Q_r, in this case, charge recombination starts to dominate the carrier processes.

For the shelf-aged device [Fig. 2(b)], the C–V and dC/dV–V curves are separated into five regions, the carrier processes in regions I–IV are identical to those in the pristine device. However, in region V, where capacitance recovery happens, $C < C_g$, charge recombination is still dominant in the carrier process. Since $dC/dV > 0$, the charge recombination rate decreases while the charge accumulation rate increases in this region. Therefore, the capacitance recovery of the shelf-aged device is associated with the change in charge accumulation and recombination rates. With the charge accumulation rate further increasing, the capacitance of the shelf-aged device can even recover to a positive value above C_g in region VI at 100 Hz (Fig. S4). In this case, Q_{acc} is larger than Q_r, the charge accumulation resumes dominance over recombination.

On the other hand, the applied voltage in the capacitance recovery region ranges from 3.1 to 5.0 V at 100 Hz, 3.9 to 5.0 V at 500 Hz, and 4.5 to 5.0 V at 1000 Hz, respectively. It coincides with the space charge limited current (SCLC) region of J–V curves. As depicted in Fig. 3(a), we separate the J–V curve of the shelf-aged device into three conduction regions. At a low bias less than 2.1 V, the current density of the shelf-aged device is linear with the working voltage, which shows Ohmic conduction. As the voltage further increases, the current density is increases sharply, showing a trap-limited conduction behavior. In this case, the current density is linear with V^m ($m = 21$, it is associated with trap distribution). Then, the current density in the J–V curve increases a little slowly, following a linear relationship with V^2, which represents space charge-limited conduction.[4] The SCLC region ranges from 3.0 to 5.0 V, which coincides with the capacitance recovery region. Therefore, it is reasonable to link the capacitance recovery behavior with the space charges in the blue QLED. When the voltage is located at the SCLC region, space charges are established on either side of the QD layer, and owing to Coulombic interaction, carrier generated by the small signal will accumulate on both sides of the QD layer, it would improve the charge accumulation rate and diminish the effect of charge recombination. Hence, the capacitance starts to recover at the SCLC region. As shown in Fig. 3(b), the current density of the blue QLED is significantly improved with shelf aging, which results from the enhanced conductivity of ETL.[8,24] For instance, the current density of the pristine device at 4.0 V is 32.11 mA/cm^2, it is found to improve to 97.64 mA/cm^2 for the shelf-aged device. Therefore, space charges are hard to build up in pristine blue QLED due to the lower current density, capacitance recovery will not take place in the pristine device.

To verify the effect of space charge on device capacitance, we test the J–V and C–V characteristics of the shelf-aged device at various temperatures. As shown in Fig. 4(a), the current density of the shelf-aged device is gradually reduced when the temperatures are decreased from 293 K (room temperature) to 253 K. For example, the current density of the shelf-aged device at 4.0 V is reduced from 97.64 to 77.24, 68.03, 61.76 mA/cm^2 when the temperature is gradually decreased from 293 to 273, 263, and 253 K, respectively. At the same time, the capacitance recovery of the shelf-aged device is gradually suppressed with decreasing temperature. As depicted in Fig. 4(b), at 293 K, the

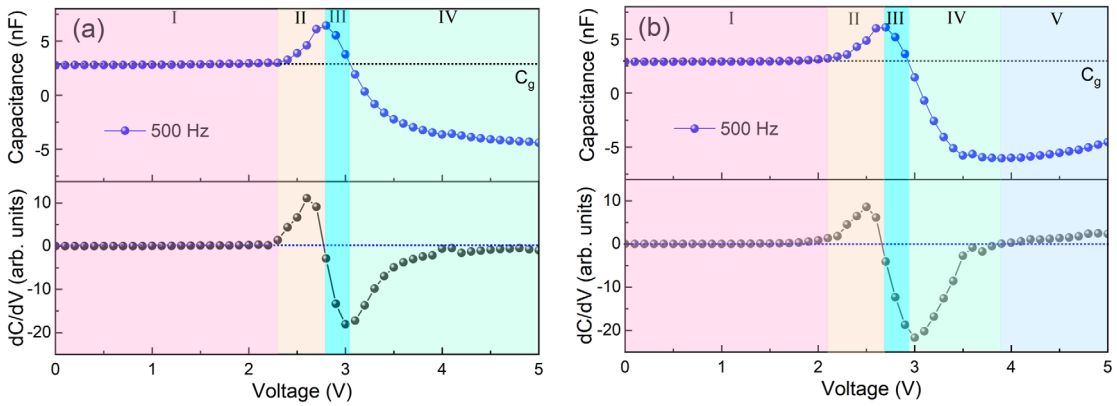

FIG. 2. Capacitance–voltage and dC/dV–V characteristics of (a) pristine and (b) shelf-aged devices at 500 Hz.

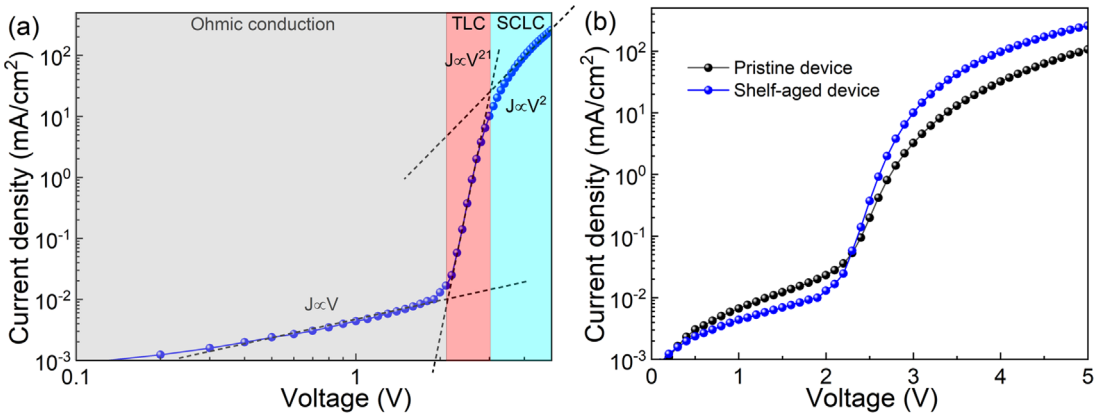

FIG. 3. (a) Current density–voltage characteristics of shelf-aged device and (b) current density–voltage characteristics of pristine and shelf-aged devices.

device capacitance recovery at 500 Hz starts at 3.6 V, and it can recover from −2.97 to −0.26 nF. As a comparison, the capacitance recovery at 273 K starts at 4.7 V, and the capacitance only recovers from −8.66 to −8.42 nF. Then, at 263 and 253 K, the capacitance recovery is nearly suppressed. Combined with J–V and C–V curves, the current density of the shelf-aged device is decreased at a low temperature as it is hard to build up the space charge in blue QLED. Therefore, the device capacitance will not rise any more. In this case, charge recombination dominates the carrier process, which consumes the carrier, thereby causing the capacitance to drop. Referring to Fig. S5, the luminance of the device conversely improves as the temperature decreases, leading to an enhancement in external quantum efficiency (EQE). We attribute it to the increased radiative recombination efficiency at low temperatures, since space charge is hard to establish in this case, which suppresses QD charging. Therefore, the capacitance recovery in blue QLED is associated with the negative device performance.

Another question relates to why the capacitance recovery behavior of the shelf-aged device only occurs at low frequencies. To interpret the frequency-related capacitance recovery behavior, we test the C–f characteristics (Fig. 5) of the shelf-aged device at the applied voltage ranging from 0 to 5.0 V. At voltage below 2.0 V, the device capacitance is almost the same as C_g, indicating little charge injection into the device. At 3.0 V, the capacitance is below C_g, and it drops as the frequency decreases, indicating charge recombination dominates the carrier process. At 4.0 and 5.0 V, the device capacitance drops first and then starts to rise as the frequency decreases. As usual, the capacitance rise is caused by charge accumulation while the capacitance drop results from charge recombination. To understand the frequency-related characteristics of capacitance recovery, it is necessary to estimate the time constants for charge accumulation and recombination at a selected voltage, as described by following equation:[16,25]

$$C(\omega) = C_g + \frac{\chi_1 C_g}{1 + (\omega\tau_{acc})^2} - \frac{\chi_2 C_g}{1 + (\omega\tau_r)^2}. \quad (2)$$

Here, $C(\omega)$ is the device capacitance, C_g is the geometrical capacitance, the second item is the increased capacitance induced by charge accumulation, the third item is the decreased capacitance caused by charge recombination. χ_1 and χ_2 are dimensionless constants, τ_{acc} and τ_r are time constants for charge accumulation and recombination, respectively, and ω is the angular frequency

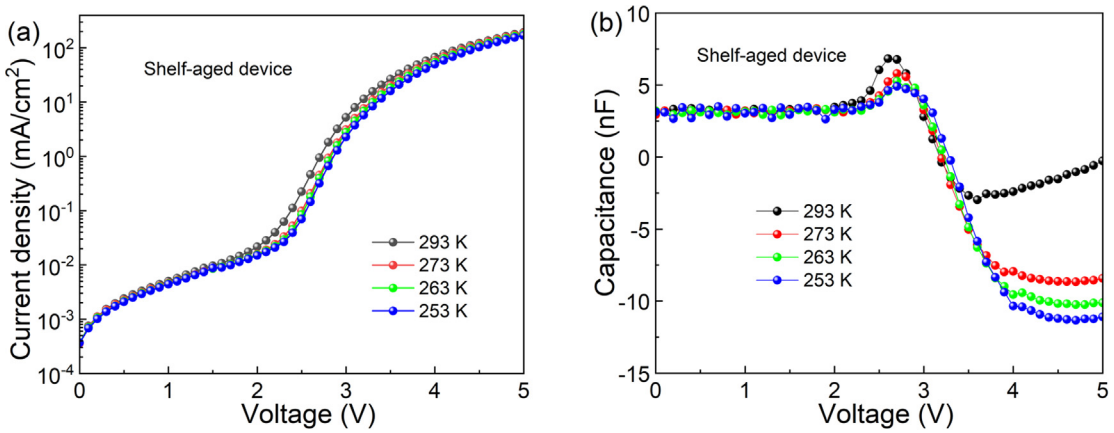

FIG. 4. (a) Current density–voltage and (b) capacitance–voltage characteristic at 500 Hz of shelf-aged device at various temperatures.

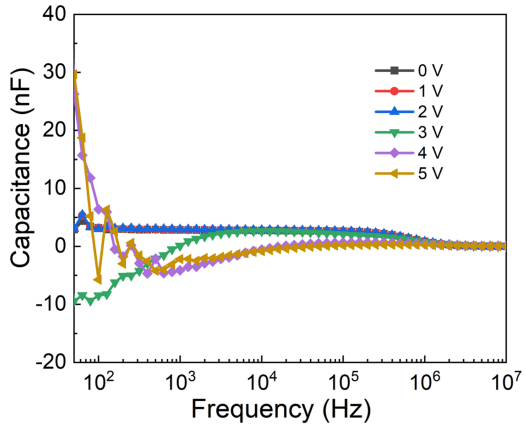

FIG. 5. Capacitance–frequency characteristics of shelf-aged device under different applied voltages.

($\omega = 2\pi f$). By fitting Eq. (2), the derived values τ_{acc} and τ_r at 4.0 V are estimated to be 1.29 and 0.028 ms (Fig. S6), respectively. Therefore, the threshold frequency for charge accumulation at 4.0 V is 772 Hz. That is to say, carriers can only follow the voltage modulation and accumulate in the device below 772 Hz. As shown in Fig. 1(b), capacitance recovery of the shelf-aged device at 4.0 V occurs at 100 and 500 Hz rather than 1 kHz, which is consistent with the C–f results. Therefore, capacitance recovery only occurs at low frequencies, it is determined by the time constant for charge accumulation at the selected voltage.

In summary, we observed the capacitance recovery of blue QLED at low frequencies. Combining with the C–V, dC/dV–V, and J–V analyses of pristine and shelf-aged devices, we show the capacitance recovery is related to space charge-induced charge accumulation. The capacitance recovery can be effectively suppressed at low temperatures, since space charges are hard to build up at low temperatures. Furthermore, capacitance recovery only happens at low frequency, which is related to the time constant for charge accumulation at the selected voltage.

See the supplementary material for details on the device structure and EL spectrum of blue QLED, J–V–L characteristics of the pristine and shelf-aged blue QLEDs, C–V curves of the pristine and shelf-aged red QLEDs, C–V and dC/dV–V characteristics of pristine and shelf-aged blue devices at 100 Hz, luminance and EQE characteristics of blue QLED at different temperatures, original and fitting data of $(C–C_g)–\omega$ characteristic at 4.0 V.

This work was supported by the National Key Research and Development Program of China (Nos. 2022YFB3602903, 2021YFB3602703, and 2022YFB3606504), the National Natural Science Foundation of China (No. 62122034), Guangdong University Key Laboratory for Advanced Quantum Dot Displays and Lighting (No. 2017KSYS007), Shenzhen Key Laboratory for Advanced Quantum Dot Displays and Lighting (No. ZDSYS201707281632549), Shenzhen Science and Technology Program (No. JCYJ20220818100411025), Shenzhen Development and Reform Commission Project (Grant No. XMHT20220114005), and High Level of Special Fund of SUSTech (No. G03034K002).

AUTHOR DECLARATIONS

Conflict of Interest

The authors have no conflicts to disclose.

Author Contributions

Xiangwei Qu: Conceptualization (equal); Data curation (equal); Formal analysis (equal); Investigation (equal); Methodology (equal); Writing – original draft (equal). **Jingrui Ma:** Investigation (equal); Methodology (equal). **Depeng Li:** Investigation (equal); Methodology (equal). **Kai Wang:** Investigation (equal); Methodology (equal). **Xiao Wei Sun:** Conceptualization (equal); Funding acquisition (equal); Project administration (equal); Resources (equal); Supervision (equal); Writing – review & editing (equal).

DATA AVAILABILITY

The data that support the findings of this study are available from the corresponding author upon reasonable request.

REFERENCES

[1]X. Dai, Z. Zhang, Y. Jin, Y. Niu, H. Cao, X. Liang, L. Chen, J. Wang, and X. Peng, Nature **515**(7525), 96–99 (2014).
[2]W. Cao, C. Xiang, Y. Yang, Q. Chen, L. Chen, X. Yan, and L. Qian, Nat. Commun. **9**, 2608 (2018).
[3]L. Qian, Y. Zheng, J. Xue, and P. H. Holloway, Nat. Photonics **5**(9), 543–548 (2011).
[4]B. S. Mashford, M. Stevenson, Z. Popovic, C. Hamilton, Z. Zhou, C. Breen, J. Steckel, V. Bulovic, M. Bawendi, S. Coe-Sullivan, and P. T. Kazlas, Nat. Photonics **7**(5), 407–412 (2013).
[5]Y. Deng, F. Peng, Y. Lu, X. Zhu, W. Jin, J. Qiu, J. Dong, Y. Hao, D. Di, Y. Gao, T. Sun, M. Zhang, F. Liu, L. Wang, L. Ying, F. Huang, and Y. Jin, Nat. Photonics **16**(7), 505–511 (2022).
[6]Y. Shirasaki, G. J. Supran, M. G. Bawendi, and V. Bulović, Nat. Photonics **7**(1), 13–23 (2013).
[7]X. Qu, W. Liu, D. Li, J. Ma, M. Gu, S. Jia, G. Xiang, and X. Sun, Nanoscale **15**(7), 3430–3437 (2023).
[8]D. Chen, D. Chen, X. Dai, Z. Zhang, J. Lin, Y. Deng, Y. Hao, C. Zhang, H. Zhu, F. Gao, and Y. Jin, Adv. Mater. **32**(52), 2006178 (2020).
[9]D. Chen, L. Ma, Y. Chen, X. Zhou, S. Xing, Y. Deng, Y. Hao, C. Pu, X. Kong, and Y. Jin, Nano Lett. **23**(3), 1061–1067 (2023).
[10]X. Qu and X. Sun, J. Semicond. **44**(9), 091603 (2023).
[11]H. Xiao, K. Wang, R. Wang, W. Chen, and K. S. Chiang, IEEE Electron Device Lett. **41**(1), 87–90 (2020).
[12]M. Zhang, F. Guo, S. Lei, T. Zhong, B. Xiao, C. Liu, L. Wang, J. Chen, Q. You, J. Liu, and R. Yang, Dyes Pigm. **195**, 109703 (2021).
[13]X. Qu, J. Ma, C. Shan, P. Liu, A. K. K. Kyaw, and X. W. Sun, Appl. Phys. Lett. **121**(11), 113507 (2022).
[14]C. Xiang, L. Wu, Z. Lu, M. Li, Y. Wen, Y. Yang, W. Liu, T. Zhang, W. Cao, S. Tsang, B. Shan, X. Yan, and L. Qian, Nat. Commun. **11**(1), 1646 (2020).
[15]X. Qu, N. Zhang, R. Cai, B. Kang, S. Chen, B. Xu, K. Wang, and X. W. Sun, Appl. Phys. Lett. **114**(7), 071101 (2019).
[16]L. Zhang, H. Nakanotani, and C. Adachi, Appl. Phys. Lett. **103**(9), 093301 (2013).
[17]V. Shrotriya and Y. Yang, J. Appl. Phys. **97**(5), 054504 (2005).
[18]J. Ma, H. Tang, X. Qu, G. Xiang, S. Jia, P. Liu, K. Wang, and X. W. Sun, Chin. Phys. Lett. **39**(12), 128401 (2022).
[19]J. Mock, M. Kallergi, E. Gross, M. Golibrzuch, B. Rieger, and M. Becherer, IEEE Photonics J. **14**(4), 8237309 (2022).

[20]S. Liang, S. Wang, Z. Wu, B. Wen, G. Cai, X. Jiang, G. Huang, C. Li, Y. Zhao, and Z. Du, Adv. Opt. Mater. **11**(2), 2201802 (2023).
[21]A. Ghorbani, J. Chen, P. Chun, Q. Lyu, G. Cotella, and H. Aziz, Small **20**(1), 2304580 (2024).
[22]D. Kim, S. Lee, J. Kim, and H. Lee, IEEE Electron Device Lett. **44**(6), 959–962 (2023).
[23]X. Qu, J. Ma, K. Wang, and X. W. Sun, Appl. Phys. Lett. **124**(26), 263503 (2024).
[24]Q. Su, Y. Sun, H. Zhang, and S. Chen, Adv. Sci. **5**(10), 1800549 (2018).
[25]C. Blauth, P. Mulvaney, and T. Hirai, J. Appl. Phys. **125**(19), 195501 (2019).